SYNTHESIS, CHARACTERIZATION, STRUCTURE-PROPERTY RELATIONSHIP AND NON-LINEAR OPTICAL (NLO) STUDIES OF HALOGENATED CHALCONES

WONG QIN AI

UNIVERSITI SAINS MALAYSIA

2025

SYNTHESIS, CHARACTERIZATION, STRUCTURE-PROPERTY RELATIONSHIP AND NON-LINEAR OPTICAL (NLO) STUDIES OF HALOGENATED CHALCONES

by

WONG QIN AI

Thesis submitted in fulfilment of the requirements
for the degree of
Doctor of Philosophy

May 2025

ACKNOWLEDGEMENT

First and foremost, I would like to extend my heartfelt gratitude to my supervisor, Assoc. Prof. Dr Quah Ching Kheng, for his unwavering support and invaluable guidance throughout the course of my research. His commitment to academic excellence and his keen insights have profoundly shaped the direction of this dissertation. I am deeply grateful for his encouragement and thoughtful feedback.

I would also like to express my sincere appreciation to Dr Parutagouda Shankaragouda Patil, Dr Shivaraj R. Maidur, Dr Kwong Huey Chong, Dr Chia Tze Shyang and Dr Yip-Foo Win for their generous teaching and guidance. Their constructive suggestions and feedback have been crucial in elevating the quality of my work.

I am thankful to the faculty and staff of the School of Physics, Universiti Sains Malaysia, for their assistance and resources, which were instrumental to the completion of this research. I am equally indebted to my fellow students, whose camaraderie and thought-provoking discussions have been a great source of inspiration and support.

Lastly, my deepest gratitude goes to my family for their unwavering encouragement, especially during difficult times. Their constant support has been invaluable, and I cannot thank them enough.

TABLE OF CONTENTS

LIST OF TABLES

Page

LIST OF FIGURES

Page

LIST OF PLATES

Page

LIST OF SCHEMES

LIST OF SYMBOLS

A	Absorbance
A	Acceptor
$\tilde{\alpha}$	Absorption coefficient
$\angle$	Angle
ω	Angular frequency
π^*	Antibonding π-orbital
H_{he}	Average degree of spatial extension of hole and electron distributions
N_{A}	Avogadro's number
$\omega(z)$	Beam radius at a given z-position along the beam
ω_0	Beam waist radius
δ	Bending mode/chemical shift
$r_{\mathrm{x-y}}$	Bond length between atoms x and y
π	Bonding π-orbital
$^{13}\mathrm{C}$	Carbon-13
C═O	Carbonyl group
C_{ele}, C_{hole}	Centroid of electron, centroid of hole
d_{CT}	Charge transfer distance
R^2	Coefficient of determination
c_i	Concentration of solution
C	Constant
n^c	c^{th} power of number of π-electrons
γ	Cubic hyperpolarizability
γ_{CPKS}	Cubic hyperpolarizability calculated by coupled-perturbed Kohn–Sham method
γ^{NI}	Cubic hyperpolarizability calculated by numerical integration method
γ_{3SM}	Cubic hyperpolarizability calculated by three-state model

$\rho^{(3)}(\vec{r})$	Cubic hyperpolarizability density
D_{as}	Density of asymmetric structure
D_{calc}	Density of unit cell
f_0	DFT-calculated oscillator strength
D	Diameter of the collimated beam at the lens
$\tilde{\mu}$	Dipole moment
d	Distance
z	Distance of the sample from the focus at Z-scan experiment
D	Donor
d	Doublet (NMR signal)
L_{eff}	Effective length of the sample
χ_{eff}	Effective susceptibility
$\tilde{E}$	Electric field
ρ	Electron density
r^2	Electronic spatial extent
σ^+	Electrophilic substituent constant
$V(r)$	Electrostatic potential
e	Elementary charge
U_{eq}	Equivalent isotropic atomic displacement parameter
σ_{ex}	Excited-state absorption cross-section
f_{exp}	Experimental oscillator strength in solution
n_4	Fifth-order non-linear refraction coefficient
R_{FOM}, W_{FOM}	Figures of merits
$F(z)$	Fluence at z-position
f	Focal length
ν	Frequency of the incident photons
S	Goodness of fit
σ_g	Ground state absorption cross-section
E_{he}	Hole-electron coulomb attractive energy
$E_{H\text{-}L}$	HOMO-LUMO gap

^{1}H	Hydrogen-1
$\Im$	Imaginary part
$\tilde{P}$	Induced dielectric polarization
P_{in}	Input power of laser
U_{iso}	Isotropic atomic displacement parameter
l	Length of cuvette
α_0	Linear absorption coefficient
n_0	Linear refractive index
$-i\rho_{iii}^{(3)}(\vec{r})$	Local contributions of cubic hyperpolarizability
L	Lorentz local field factor
m_e	Mass of electron
λ_{abs}	Maximum absorption wavelength
θ_{max}, θ_{min}	Maximum and minimum theta angle in degrees for the measured intensities
T_{max}, T_{min}	Maximum and minimum transmission factors applied to the diffraction pattern
$\Delta\rho_{max}$, $\Delta\rho_{min}$	Maximum and minimum values of the electron density in the final difference Fourier map.
ε	Molar absorptivity
N_c	Molecular number density in unit volume
m	Multiplet (NMR signal)
n	Nonbonding orbital
α_2	Non-linear absorption coefficient/ two-photon absorption coefficient
$\Delta\phi_{NL}$	Non-linear phase shift
n_2	Non-linear refractive index coefficient/ third-order non-linear refraction coefficient
T_{OA}	Normalized transmittance for closed-aperture Z-scan
T_{CA}	Normalized transmittance for open-aperture Z-scan
$\chi^{(n)}$	n^{th}-order susceptibility
N	Number of data points

N_{rot}	Number of single bonds of molecule that are free to rotate
$K^{(n)}$	Numerical factor
F_0	On-axis fluence at focus
P_0	On-axis peak power
F_{on}	Onset optical limiting
E_g	Optical gap
F_{th}	Optical limiting threshold
$\frac{dI}{dz'}$	Optical loss
Θ_{ID}	Ovality index
$\Delta\sigma_{he}$	Overall difference between RMSD of hole and electron
F	Overall statistical significance of the equation
S_r	Overlap degree of hole-electron distribution
I_0	Peak irradiance
r_{xy}	Pearson correlation coefficients
$p_{exp,dft}$	Percentage difference of wavelength between experimental and theoretical results
μ	Permanent dipole moment
$\Delta\mu$	Permanent dipole moment difference between ground and excited states
μ_{ee}	Permanent dipole moment in the excited state
μ_{gg}	Permanent dipole moment in the ground state
ε_0	Permittivity of free space
$\frac{d\Delta\phi}{dz'}$	Phase shifts
h	Planck's constant
A_{pol}	Polar surface area
α	Polarizability
$\vec{r}$	Position vector
z'	Propagation length inside the sample
E_p	Pulse energy
τ_p	Pulse width

β	Quadratic hyperpolarizability
z_R	Rayleigh length
$\Re$	Real part
n	Refractive index
f_{rep}	Repetition rate
$R[F^2 > 2\sigma(F^2)]$	Residual factor for the reflections judged significantly intense and included in the refinement.
t_{he}	Separation degree of hole-electron in charge transfer direction
s	Singlet (NMR signal)
$S_0 \rightarrow S_n$	Singlet-singlet excitation from ground state to n^{th} excited state
m	Slope
c	Speed of light
z-score	Standard deviations from the mean
$\rho(X)$	Steric density parameter of substituents
v	Stretching mode
$F(000)$	Structure factor evaluated in the zeroth-order case $h = k = l = 0$
X	Substituent
Z	The numbers of the formula units in the unit cell
R_{int}	The residual for the sum of the average absolute differences between the average intensity and the individual symmetry-equivalent intensities, divided by the sum of the average intensity for symmetry-equivalent reflections
α_3	Three-photon absorption coefficient
I	Time-averaged intensity
μ_{eg}	Transition dipole moment from the ground state to first-singlet excited state
v_{eg}	Transition frequency between ground state to first excited state
ΔT_{p-v}	Transmittance difference between peak-valley of the closed-aperture Z-scan curve
t	Triplet (NMR signal)
σ_{2PA}	Two-photon absorption cross-section

A_{vdW}	*Van der Waals* surface area
V_{as}	Volume of asymmetric structure
V	Volume of unit cell
k	Wave vector
λ	Wavelength
$\Delta\lambda_{abs}$	Wavelength shift
$\tilde{\nu}$	Wavenumber of UV-Vis light
$wR(F^2)$	Weighted residual factors for all reflections included in the refinement.
w: A, B	Weighting scheme
Δz_{p-v}	z-position difference between peak-valley of the closed-aperture Z-scan curve

LIST OF ABBREVIATIONS

1PA	One-photon absorption
2PA	Two-photon absorption
2SM	Two-state model
3PA	Three-photon absorption
3SM	Three-state model
AATCM	Atom-atom charge transfer matrix
ACRHEM	Advanced Centre of Research in High Energy Materials
AI	Artificial intelligence
AIM	Atoms-in-molecules
A-ring	Aromatic ring that bridged to the carbonyl group
ATR	Attenuated total reflection
B3LYP	Becke, 3-parameter, Lee-Yang-Parr exchange-correlation functional
BC	Benzoyl chalcone
BLA	Bond-length alteration
B-ring	Aromatic ring that bridged to the vinyl group
CA	Closed-aperture
CAM-B3LYP	Coulomb-Attenuated Method B3LYP
Cbz	9*H*-carbazol-9-yl moiety
CCD	Charge-Coupled Device
CCl_4	Carbon tetrachloride
CCSD	Coupled Cluster Singles and Doubles
$CDCl_3$	Deuterated chloroform
Cg	Centroid
Ch	Chalcone skeleton
CPCM	Conductor polarizable continuum model
CPKS	Coupled-perturbed Kohn–Sham
cSAR	Charge of the substituent active region

CSD	Cambridge structural database
CT	Charge transfer
CW	Continuous wave
DC-KE	DC-Kerr effect
DFT	Density functional theory
DFWM	Degenerate four-wave mixing
DMF	*N*, *N*-Dimethylformamide
DMSO	Dimethyl sulfoxide
ED	Electron-donating
EDG	Electron-donating group
ELF-π	Electron-localization function-π
EOPE	Electro-optic Pockels effect
ESA	Excited-state absorption
EFISH	Electric-field-induced second harmonic generation
ESP	Electrostatic potential
EW	Electron-withdrawing
EWG	Electron-withdrawing group
FF	Finite-field
FWHM	Full width at half maximum
FMO	Frontier molecular orbital
FOM	Figure of merit
FTIR	Fourier-transform infrared
GAc	Guanidium acetate
HAR	Hirshfeld atom refinement
HF	Hartree-Fock
HMQC	Heteronuclear multiple quantum coherence
HOMA	Harmonic oscillator measure of aromaticity
HOMO	High occupied molecular orbital
HRS	Hyper-Rayleigh scattering
IDRI	Intensity-dependent refractive index

IEFPCM	Integral equation formalism-polarizable continuum model
IFCT	Interfragment charge transfer
IR	Infrared
LE	Local excitation
LMO	Localized molecular orbital
LSP	Least-square planes
LUMO	Low unoccupied molecular orbital
M06	Minnesota 2006 hybrid functional
MCBO	Multicenter bond order
Me	Methyl
MeCN	Acetonitrile
MLR	Multiple linear regression
MM	Molecular mechanics
MP2	Møller-Plesset second-order perturbation theory
MPA	Multiple-photon absorption
MPI	Molecular polarity index
MPP	Molecular planarity parameter
NBO	Natural bond orbital
NLA	Non-linear absorption
NLO	Non-linear optical/ non-linear optics
NLR	Non-linear refraction
NMe_2	Dimethylamino
NMR	Nuclear magnetic resonance
NPA	Natural population analysis
OA	Open-aperture
ODI	Orbital delocalization indices
OKE	Optical Kerr effect
OMe	Methoxy
OR	Optical rectification
ORTEP	Oak ridge thermal-ellipsoid plot

PBE0	Functional Mixes the Perdew-Burke-Ernzerhof (PBE) exchange energy and 25% Hartree-Fock exchange energy, along with the full PBE correlation energy
PBE38	Functional Mixes the Perdew-Burke-Ernzerhof (PBE) exchange energy and 37.5% Hartree-Fock exchange energy, along with the full PBE correlation energy
PCM	Phase-change material
pEDA	π-electron donor-acceptor
PERC	Tetrachloroethene
PICT	Planar intramolecular charge transfer
QCC	Quantum chemical calculation
QM	Quantum mechanics
QSPR	Quantitative structure-property relationship
RMSD	Root-mean-square deviation
RSA	Reverse saturable absorption
SA	Saturable absorption
SADABS	Siemens Area Detector Absorption Correction
SAINT	SAX Area Detector Integration
SCXRD	Single-crystal X-ray Diffraction
SD	Standard deviation
SE	Substituent effect
sEDA	σ-electron donor-acceptor
SHG	Second harmonic generation
SMART	Siemens Molecular Analysis Research Tools
SOS	Sum-over-states
SPR	Structure-property relationship
TC	3-Thienoyl chalcone
TCM	Chloroform
TD-DFT	Time-dependent Density Functional Theory
TD-HF	Time-dependent Hartree-Fock
THF	Tetrahydrofuran

THG	Third harmonic generation
TICT	Twisted intramolecular charge transfer
TLC	Thin layer chromatography
TMS	Tetramethylsilane
UM	Universiti Malaya
USM	Universiti Sains Malaysia
UTAR	Unversiti Tunku Abdul Rahman
UV	Ultraviolet
VAC	Vacuum
vdW	*Van der Waals*
Vis	Visible
VMD	Visual molecular dynamic

LIST OF APPENDICES

SINTESIS, PENCIRIAN, HUBUNGAN STRUKTUR-SIFAT DAN KAJIAN OPTIK TAK LINEAR (NLO) KALKON BERHALOGEN

ABSTRAK

Pengaruh pengganti penarik elektron (EW) dan penderma elektron (ED) terhadap terbitan kalkon yang berkenaan dengan sifat-sifat fotofisikal dan optik tak linear (NLO) tertib ketiga telah dikaji secara komprehensif menggunakan gabungan kaedah eksperimen dan teori. Tiga siri dengan sejumlah sebelas sebatian kalkon berhalogen, termasuk kalkon berasaskan tienoil dan benzoil, telah direka dan disintesis. Pencirian dilakukan menggunakan spektroskopi FTIR dan NMR, manakala struktur hablur dikaji menggunakan analisis SCXRD. Kajian kuantum-kimia memperkenalkan bahawa perubahan sifat elektronik dipacu oleh kesan penggati, termasuk sifat ED/EW, penyahsetempatan elektron, kearomatikan dan kekutuban. Terbitan dengan EDG yang kuat dan sistem gelang yang diperluas menunjukkan kekutuban molekul yang lebih tinggi, penyelangan panjang ikatan (BLA) seperti sianina di bahagian enon, dan jurang tenaga HOMO-LUMO yang lebih sempit (< 3.7 eV). Spektroskopi penyerapan UV-Vis mengesahkan kelutsinaran yang meluas (> 500 nm) pada semua terbitan, menandakan kesesuaiannya untuk aplikasi optik. Analisis lubang-elektron, spektrum IFCT dan peta haba AATCM memperkenalkan mekanisme pengujaan yang dipengaruhi oleh kedudukan pengganti. Pengganti EDG pada kedudukan para di gelang B memudahkan penyahsetempatan electron yang berjarak jauh, manakala halangan sterik daripada pengganti berhampiran titian π-konjugasi melemahkan penyahsetempatan cas. Kesan ini menyumbang kepada pergeseran auksokromik, memodulasi tenaga pengujaan (E_{ex} = 3.2–4.1 eV) dan momen dwikutub peralihan (μ_{eg} = 3.7–10.1 D) secara langsung dalam siri kalkon. Kedua-dua parameter

tersebut sejajar dengan ramalan model dua-peringkat bagi hiper-keterkutuban, dan dengan itu mengesahkan modulasi sifat NLO yang bergantung pada pengganti. Respons NLO tertib ketiga, berkaitan dengan indeks biasan yang bergantung pada keamatan, telah diukur melalui teknik imbasan-Z dengan laser berdenyut femtosaat 800 nm. Keputusan mengesahkan penyerapan dua-foton (2PA) ($\alpha_2 \approx 10^{-12}$ cm·W^{-1}) dan kesan fokus diri ($n_2 \approx 10^{-17}$ cm^2·W^{-1}), yang berasal daripada polarisasi elektronik. Sebatian **T2**, **B7** and **F7** menunjukkan pembatasan optic yang luar biasa (F_{th}: 9.48–13.99 mJ·cm^{-2}), mencadangkan potensinya sebagai pembatas optic. Sementara itu, sebatian **B6** mempamerkan nisbah NLR kepada NLA tertinggi dan kehilangan penyerapan linear yang rendah, menjadikannya calon untuk aplikasi suis optik sepenuhnya. Pengiraan komputer CPKS bagi hiper-keterkutuban padu ($\gamma \approx 10^{-34}$ esu) sejajar dengan data eksperimen dan berkorelasi dengan kekuatan ED pengganti, yang dipacu oleh pengagihan cas tak simetri dan pemindahan cas berkesan dari kedua-dua gelang aromatik ke arah kumpulan karbonil. Kesan penggantian ED terhadap hiper-keterkutuban padu dianalisis lanjut menggunakan analisis penguraian hiper-keterkutuban padu. Model perhubungan kuantitatif struktur-sifat (QSPR) yang diperoleh melalui regresi linear berganda (MLR) menunjukkan korelasi yang kuat dengan hiper-keterkutuban padu dinamik yang diukur secara eksperimen. Hasil kajian mengesahkan bahawa corak pengganti, geometri molekul, kekutuban, kearomatikan, dan pemindahan cas mengawal respons NLO terbitan kalkon. Penemuan ini menjelaskan bagaimana faktor struktur dan elektronik saling bergantung dalam menentukan sifat NLO, dengan demikian menyediakan rangka kerja untuk reka bentuk rasional molekul dengan fungsi optik tersuai secara rasional.

SYNTHESIS, CHARACTERIZATION, STRUCTURE-PROPERTY RELATIONSHIP AND NON-LINEAR OPTICAL (NLO) STUDIES OF HALOGENATED CHALCONES

ABSTRACT

The influence of electron-withdrawing (EW) and electron-donating (ED) substituents on chalcone derivatives concerning the photophysical and third-order non-linear optical (NLO) properties was comprehensively studied using a combination of experimental and computational approaches. Three series with a total of eleven halogenated chalcone compounds, which include thienoyl- and benzoyl-based chalcones, were designed and synthesized. Characterization was performed using FTIR and NMR spectroscopies, whereas crystal structures were investigated using SCXRD analysis. Quantum-chemical studies revealed that changes in electronic properties are driven by substituent effects, including ED/EW character, electron delocalization, aromaticity and polarity govern. Derivatives with strong EDGs and extended ring system exhibited higher molecular polarity, cyanine-like bond length alternation (BLA) in enone moiety and narrower HOMO-LUMO gap (< 3.7 eV). UV-Vis absorption spectroscopy confirms broad transparency (> 500 nm) across all derivatives, indicating their suitability for optical applications. Hole-electron analysis, IFCT spectrum and AATCM heat map revealed excitation mechanisms governed by substituent positioning. *Para*-substituted EDGs on B-ring facilitated long-distance electron redistribution, whereas steric hindrance from substituents proximal to π-conjugation bridge weakened charge delocalization. These effects contribute to the auxochromic shift, directly modulating excitation energy (E_{ex} = 3.2–4.1 eV) and transition dipole moment (μ_{eg} = 3.7–10.1 D) across the chalcone series. Both

parameters align with the two-state model's prediction of (hyper)polarizability, thereby validating the substituent-dependent modulation of NLO behaviour. Third-order NLO responses, related to intensity-dependent refractive index, were measured through Z-scan technique with 800 nm femtosecond pulsed laser. The results showed two-photon absorption (2PA) ($\alpha_2 \approx 10^{-12}$ cm·W^{-1}) and self-focusing effects ($n_2 \approx 10^{-17}$ cm^2·W^{-1}), which originated from electronic polarization. Compounds **T2**, **B7** and **F7** demonstrated exceptional optical limiting (F_{th}: 9.48–13.99 mJ·cm^{-2}), indicating their potential application for optical limiters. Meanwhile, compound **B6** exhibited the highest NLR to NLA ratio and low linear absorption loss, making it a candidate for all-optical switching applications. Computational CPKS calculations of cubic hyperpolarizability ($\gamma \approx 10^{-34}$ esu) matched experimental data and correlated with ED strength of the substituent, driven by asymmetric charge distribution and effective charge transfer from both aromatic rings toward the carbonyl group. The impact of ED substitution on cubic hyperpolarizability was further analyzed using cubic hyperpolarizability decomposition analysis. A quantitative structure-property relationship (QSPR) model, derived from multiple linear regression (MLR), showed a strong correlation with experimentally measured dynamic cubic hyperpolarizability. The results confirmed that substitution patterns, molecular geometry, polarity, aromaticity, and charge transfer properties collectively govern the NLO behaviour of chalcone derivatives. These findings elucidate how structural and electronic factors interdependently dictate the NLO properties, providing a framework for the rational design of molecules with tailored optical functionalities.

CHAPTER 1

INTRODUCTION

1.1 Overview of Research Project

Non-linear optical (NLO) materials are crucial in photonics and optoelectronics due to their numerous potential applications in optical computing and communication, *e.g.*, signal processing, optical limiting, ultrafast switching, and optical data storage. Optical switching, a key NLO property, holds promise for revolutionary optical computers, while optical storage devices can read and write information at much higher speeds (Chai *et al.*, 2017; Li, 2017). Additionally, halving the wavelength of the laser light used in these devices can quadruple their storage capacity. NLO materials also excel at changing the frequency of the light source, making them exceptional mediums for various applications (Kim *et al.*, 2021).

Researchers in photonics and optoelectronics recognize the importance of exploring new organic NLO crystals and understanding the relationship between their crystal structure and NLO properties. These materials have gained significant attention since the discovery of phenomena such as optical second harmonic generation (SHG) (Barhum *et al.*, 2023), third harmonic generation (THG) (Fuentes-Hernandez *et al.*, 2009), and optical Kerr effect (Perry *et al.*, 2010) due to their wide range of applications. Devices utilizing these materials dissipate less heat and respond in nearly femtoseconds, contributing to further miniaturization of computing circuits. NLO crystals play a vital role in laser science and engineering, with ongoing active research to discover new NLO crystals, particularly organic compounds, in the ultraviolet (UV) and infrared (IR) spectral regions (Huang *et al.*, 2022; Luo *et al.*, 2019). Despite intensive efforts, designing and synthesizing organic compounds with versatile optical

properties remains challenging. The development of optical devices, such as photonic integrated circuits, strongly depends on the design of highly efficient NLO materials.

Considering that the NLO properties are influenced by charge transfer (CT) processes and dipole moment within the molecules, our approach to preparing chalcone samples is based on the following ideas. The push-pull configuration of the chalcone contributes to the intramolecular CT, which can be tuned by altering the positions and strength of the electron-withdrawing (EW) and electron-donating (ED) substituents on the two terminal rings. Meanwhile, intermolecular charge transfer can be influenced by the crystal packing aggregations, which can be determined *via* single crystal X-ray diffraction (SCXRD) techniques. The photophysical and ultrafast third-order NLO properties are studied using UV-Vis absorption spectroscopy and ultrafast femtosecond Z-scan technique, respectively. The mechanism of intramolecular charge transfer and hyperpolarizabilities are further quantified using Density Functional Theory (DFT). The relationship between structure and NLO properties is examined and a guideline for the molecular design of push-pull chalcone setup with favourable NLO properties for third-order NLO applications is developed.

1.2 Problem Statement

Optical devices, which use pulses of light instead of electrical signals, offer the potential for significantly faster signal transmission due to the inherent speed of light. As advancements in conventional electronic devices have stagnated, the demand for ultrafast computing and transmission speed driven by artificial intelligence (AI) is spurring the development of optical technologies for data transmission and information computing. However, achieving ultrafast optical data processing on integrated photonic chips requires the development of ultrafast optical switches.

Recent optical switches, including electro-optical switches (Li *et al.*, 2020), acousto-optical switches (Li *et al.*, 2019), and magneto-optical switches (Zhang *et al.*, 2022), show promise but face challenges such as slow switching speeds, heat generation, and low signal-to-noise ratio. To address these issues, the evolution of ultrafast all-optical devices operating on the femtosecond time scale is essential.

Besides, most industrial electronic, photonic, and electro-optical devices are fabricated from inorganic materials, yet several issues persist. Plasmonic structures made of metals, such as gold, have high power consumption due to Ohmic loss in the metallic material (Kuznetsov *et al.*, 2016; Tuong *et al.*, 2013) and high thermal conductivity, which negatively affects the non-linear refractive index (n_2) (Sarkhosh *et al.*, 2015). Phase-change materials (PCMs) like chalcogenide (Ge-Sb-Te system) suffer from low longevity and reliability due to the material degradation after cycling phase-changes, specifically oxidation that alters the chemical composition (Martin-Monier *et al.*, 2022). They also experience excessive losses due to free carrier absorption (González-Hernández *et al.*, 1995; Prabhathan *et al.*, 2023). Bulk lithium niobate ($LiNbO_3$) crystals face limitations, *e.g.*, low refractive index contrast, limited area of frequency conversion, and large device size (Chen *et al.*, 2022), although thin-film $LiNbO_3$ has mitigated some drawbacks. However, challenges remain, including the costly and difficult fabrication of high-quality thin films (Sumets, 2018), the photorefractive effect that decreases the refractive index (Boes *et al.*, 2023; Kong *et al.*, 2020), and integration difficulties with other materials (Chen *et al.*, 2022; Xie *et al.*, 2024).

The development of a reliable and faster optical switch with simpler preparation processes and lower energy loss remains elusive. Therefore, organic NLO materials have emerged as promising alternatives due to their structural flexibility,

ease of growing large crystals, ultrafast responses, high laser damage thresholds, low manufacturing costs, and wide range of operating frequencies (Haque *et al.*, 2010; Huang *et al.*, 2022; Wang *et al.*, 2023a; Wu *et al.*, 2020). NLO properties in organic materials are influenced by various factors, including structural geometry, electron nature of the substituent, aggregation effects, and aromaticity. The combined impact of these structural variations on NLO properties is not well understood, making it difficult to design and fabricate organic NLO compounds with tuneable optical features suitable for industrial applications.

To address this limitation, this thesis aims to identify a comprehensive set of molecular descriptors that contain diverse chemical information relevant to the NLO response for chalcone derivatives and to establish correlations between these parameters and NLO properties systemically. A better understanding of the contribution of local factors to optical properties and structure-property relationship (SPR) can guide the design of new molecules with targeted NLO properties. This knowledge gap has sparked significant research interest in developing highly efficient organic NLO materials, exploring CT mechanisms, and investigating SPR in both optical and electronic materials to meet future technological needs (Abid *et al.*, 2023; Lin *et al.*, 2022; Semin *et al.*, 2021). Establishing clear guidelines for the molecular design of organic materials with desirable NLO properties through combined experimental and theoretical approaches is essential.

1.3 Research Questions

NLO is a rapidly growing field that covers a wide range of materials and scales, from inorganic to organic, and from micrometer to nanometer dimensions. It integrates classical and quantum principles, making it an interdisciplinary research domain with

concepts that go beyond the discipline boundaries. However, NLO research has not yet reached its full potential, and several unresolved research questions remain. One area of interest is how to design chalcone compounds with optimal NLO properties by considering the push-pull effect, which is influenced by the strength and positions of the EW and ED groups. Another question to investigate is the role of efficient CT in understanding the relationship between structural variations and NLO properties.

1.4 Hypotheses

The hypotheses are as follows,

i. the design of organic chalcone compounds possessing stronger non-linearities relies on the effectiveness of π-conjugation and the strength of donor and acceptor substituents on both terminal rings, and
ii. the contribution of the behaviour of intramolecular charge transfers in the chalcone push-pull setup can be understood by combining quantum chemical calculations with ultrafast femtosecond Z-scan experimental data.

1.5 Objectives

The objectives of this research include:

1. To synthesize and characterize chalcone derivatives substituted with electron-donating group (EDG) or electron-withdrawing group (EWG) on both rings, and to determine the crystal packing of these compounds using SCXRD method.
2. To investigate the photophysical and ultrafast third-order NLO properties by UV-Vis absorption spectroscopy and femtosecond Z-scan technique.

3. To examine the impact of substituents on electronic structure and aromaticity, and their influence on the mechanism of intramolecular charge transfer, using computational molecular modelling *via* DFT.
4. To explore the relationship between substituent-driven structural modifications and the dynamic cubic hyperpolarizability, based on key electronic descriptors of the compounds.

1.6 Outlines

This thesis is organized as follows:

Chapter 1 outlines the overview of the research project by briefly introducing the NLO responses. This chapter also presents the problem statement along with the research questions and hypotheses, as well as the objectives of the project to address the research gap. This exploration combines experimental measurements with computational calculations.

Chapter 2 offers a detailed literature review focusing on the impact of structural variations, particularly within organic conjugated systems, on mechanisms of CT, photophysical properties, and NLO responses. It also provides a comprehensive introduction to NLO, covering its development, theoretical foundations, and the practical aspects of measuring the third-order NLO response. Additionally, we discuss general computational methods used to predict (hyper)polarizabilities and highlight the significance of quantum-chemical descriptor analyses in studying SPR.

Chapter 3 outlines the methodology employed in this research project, including sample preparation such as synthesis and crystallization, structure characterization *via* spectroscopy techniques, including Fourier-transform infrared (FTIR) and nuclear magnetic resonance (NMR), crystal structure determination *via*

single-crystal X-ray diffraction (SCXRD), photophysical and NLO responses analyses *via* UV-Vis and Z-scan experiment, and quantum-theoretical molecular modelling *via* DFT.

Chapter 4 presents the results of structural analyses conducted through FTIR and NMR spectroscopy as well as crystal packing using SCXRD data. This chapter also provides detailed theoretical investigations into the effects of substituents on electronic structure and aromaticity. Furthermore, it explores photophysical and NLO properties through both experimental measurements and theoretical analyses, followed by a discussion on SPR.

Finally, chapter 5 concludes this research project by summarizing the findings and highlighting avenues for future research.

CHAPTER 2

RESEARCH BACKGROUND AND LITERATURE REVIEW

2.1 Discover Non-linear Optics

NLO is a phenomenon where the polarization of a medium behaves non-linearly and differently than expected for linear polarization under intense coherent light irradiation. The NLO medium can alter the fields of the input source in terms of phase, frequency, or amplitude. The development of NLO phenomenon is credited to Bloembergen, who led the groundwork in 1965 on the interactions between light and matter (Armstrong *et al.*, 1962; Bloembergen, 1963, 2000). Bloembergen shared the Nobel Prize in Physics in 1981 with Schawlow and Siegbahn, in recognition of their contributions to the development of laser spectroscopy and high-resolution electron spectroscopy, respectively.

Before that, the phenomenon of two-photon absorption (2PA), an optical process related to an imaginary third-order non-linear susceptibility, was postulated by Göppert-Mayer (1931) and experimentally validated by Kaiser *et al.* (1961), following the invention of the first laser by Maiman (1960). The SHG phenomenon was then observed on single-crystal quartz by Franken *et al.* (1961). Various factors like frequency, polarization, phase, and path of incident light can influence NLO response (Bloembergen, 1996). From the 1960s onwards, evaluations of numerous NLO processes (Bass *et al.*, 1962; Eckhardt *et al.*, 1962; Harris *et al.*, 1967; Lallemand *et al.*, 1965) had propelled advancements in diversified NLO research fields revolutionizing state-of-art technologies, *e.g.*, frequency conversion (Mutailipu *et al.*, 2023), quantum computing (Liu *et al.*, 2008), high-resolution spectroscopy (Batignani *et al.*, 2024; Zhang *et al.*, 2024b), optical data storage (Gindre *et al.*, 2013; Kawata *et al.*, 2000) *etc*.

2.2 Literature Review

Chalcone, an organic compound known for its asymmetry and conjugated structure, along with a push-pull effect driven by the strong EW carbonyl group at the molecule's centre, has gained prominence as a NLOphores. The distinctive structural features of chalcone make them highly tuneable by introducing various functional groups such as ED or EW substituents, enabling researchers to tune their NLO properties for specific applications. Over the past decades, extensive studies in searching for a chromophore, including the chalcone derivatives, that possess strong NLO properties and optimal transparency within the visible light spectrum (Maragatham *et al.*, 2019; Sandhya *et al.*, 2020; Valverde *et al.*, 2018b). Notably, the absence of symmetry requirements for third-order NLO effect aroused considerable interest in exploring chalcone derivatives for third-order NLO. In addition to the distinct NLO processes that occur when interacting with multiple lasers, the magnitude of third-order NLO is governed by experimental conditions used, environmental factors, and structural characteristics of chalcone molecules. These experimental conditions and environmental factors complicate the comparison of third-order NLO data across different reported structures.

2.2.1 Laser Type and Z-scan Experimental Setup Conditions

The type of laser used, whether continuous wave or pulsed, significantly impacts the NLO behaviour, with variations in cubic hyperpolarizability exceeding ~10^{-8} esu (Figure 2.1) (Haleshappa *et al.*, 2019; Mathew *et al.*, 2019). Additionally, the pulse duration of the input laser induces distinct non-linear processes. For example, in dimethylamino-bis-chalcone (**C1**), a transition from saturable absorption (SA) to reverse saturable absorption (RSA) and a shift from self-focusing to self-defocusing

effects were observed when excited by femtosecond and picosecond pulses (Figure 2.2) (Yang *et al.*, 2020). These findings demonstrate the changes in non-linear absorption, including transitions between SA, 2PA, and excited-state absorption (ESA), as well as the changes in non-linear refraction, which are influenced by factors such as electrostatic polarization, molecular reorientation, and thermal effects. NLO responses, particularly SHG and 2PA, are often enhanced when near the resonance wavelengths of electronic transitions in the chalcone derivatives (Figures 2.3–2.5) (Araújo *et al.*, 2023; Chen *et al.*, 2023; Maidur *et al.*, 2017). Furthermore, higher-order non-linear refraction (*i.e.* fifth-order NLO) and non-linear absorption (*i.e.* 3PA with ESA) emerge in the chalcone derivative during femtosecond Z-scan experiment when input irradiance exceeds the critical intensity (I_c) (Figure 2.6) (Gu *et al.*, 2009b; Gu *et al.*, 2010a). NLA response gradually increases as the incident light energy increases, implying the involving ESA in the photophysical mechanism (Figure 2.7) (Jia *et al.*, 2020).

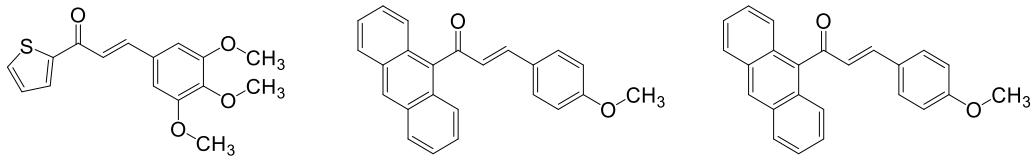

Figure 2.1 Scheme for molecular structures of **TTMP**, **Methoxy-ANC**, and **Ethoxy-ANC**[1].

[1] Using 532 nm Z-scan experiment, cubic hyperpolarizability of compounds **TTMP** is 7.02×10^{-27} esu under CW laser, whereas that of **Methoxy-ANC** and **Ethoxy-ANC** are $12.94–18.00 \times 10^{-36}$ and $23.55–40.54 \times 10^{-36}$ esu under 5 ns pulsed laser.

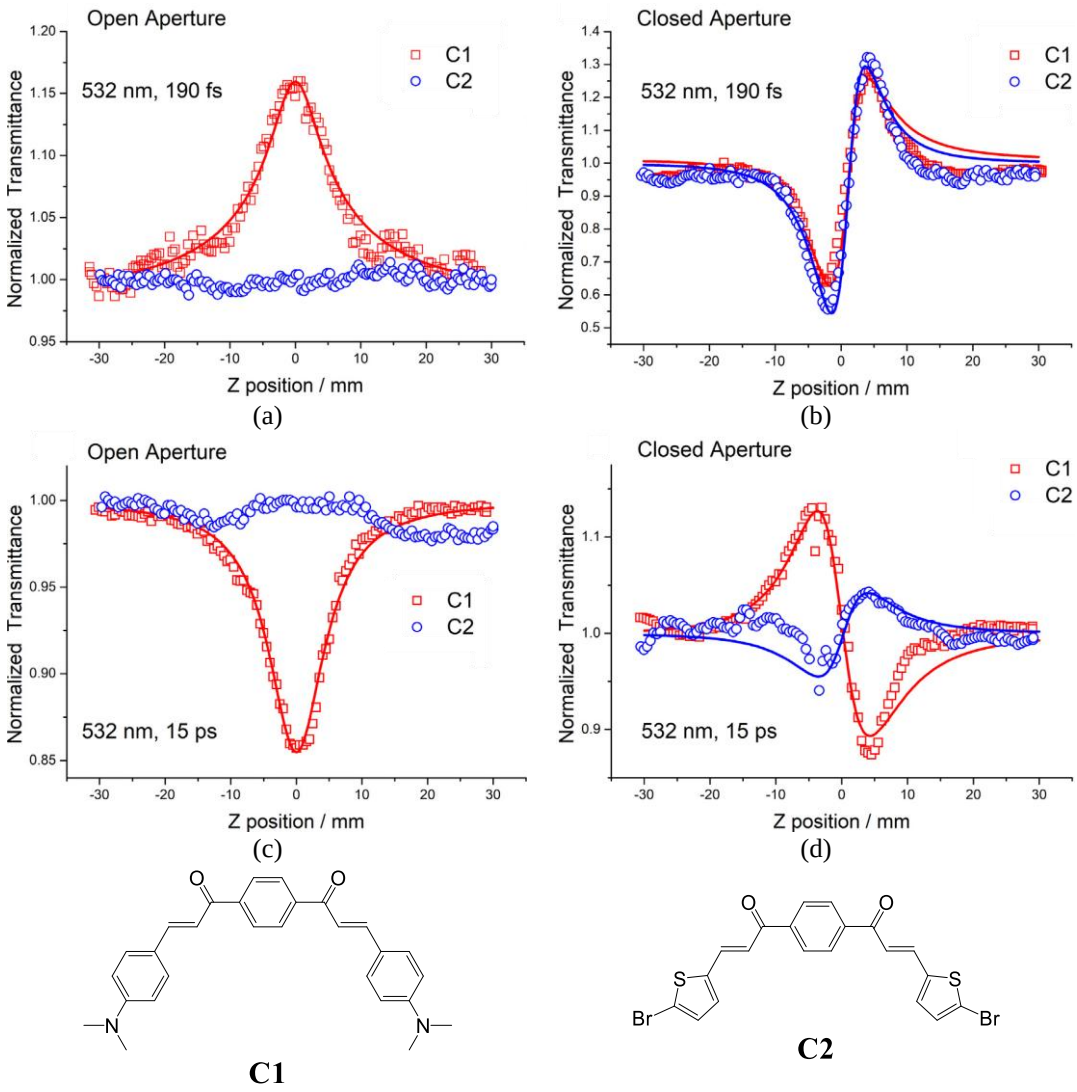

Figure 2.2 Z-scan results for compounds **C1** and **C2** under (a)(b) 190 fs and (c)(d) 15 ps pulses, respectively. (e) Scheme for molecular structures of **C1** and **C2**.

Note. Figures (a–d) adapted from reference (Yang *et al.*, 2020).

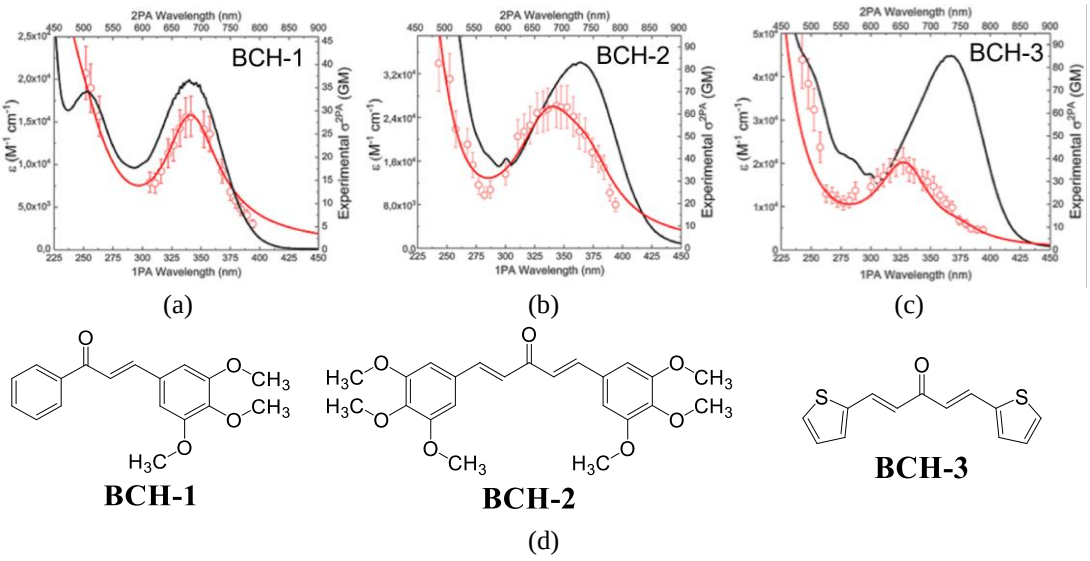

Figure 2.3 Combined plot of 2PA (red circles) and one-photon absorption (1PA) (black solid line) as well as (d) scheme for molecular structures of **BCH-1**, **BCH-2**, and **BCH-3**.

Note. 1PA and 2PA were collected through UV-Vis spectroscopy and 120 fs pulse laser Z-scan technique, respectively. Figures (a–c) adapted from reference (Araújo *et al.*, 2023).

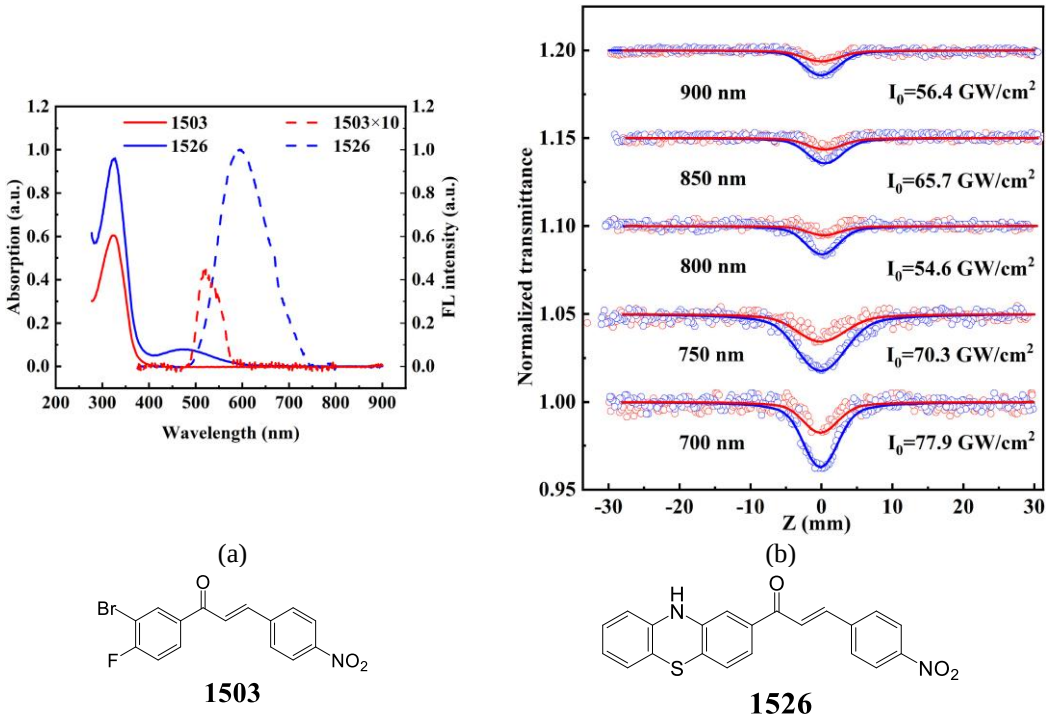

Figure 2.4 (a) UV-Vis absorption (solid line) and fluorescence (dashed line) spectrum, (b) open-aperture Z-scan results at distinct wavelengths, and (c) scheme for molecular structures of **1503** and **1526**.

Note. Z-scan experiment was performed using 190 fs pulse laser. Figures (a–b) adapted from reference (Chen *et al.*, 2023).

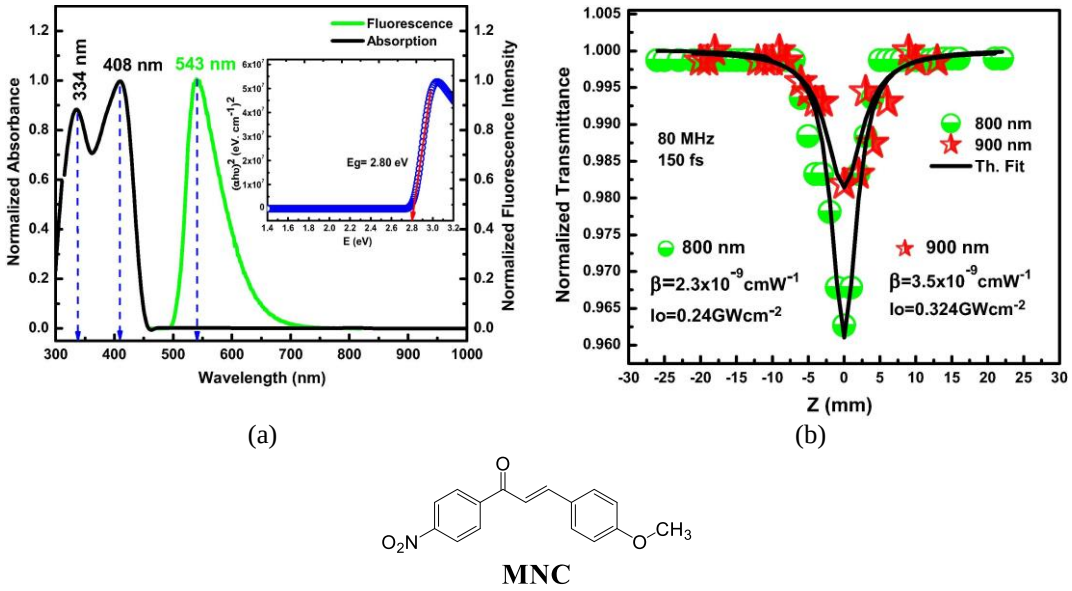

(a) (b)

MNC

(c)

Figure 2.5 (a) UV-Vis absorption and fluorescence spectrum, (b) open-aperture Z-scan results at 800 and 900 nm, and (c) scheme for molecular structure of **MNC**.

Note. Z-scan experiment was performed using 150 fs pulse laser. Figures (a–b) adapted from reference (Maidur *et al.*, 2017).

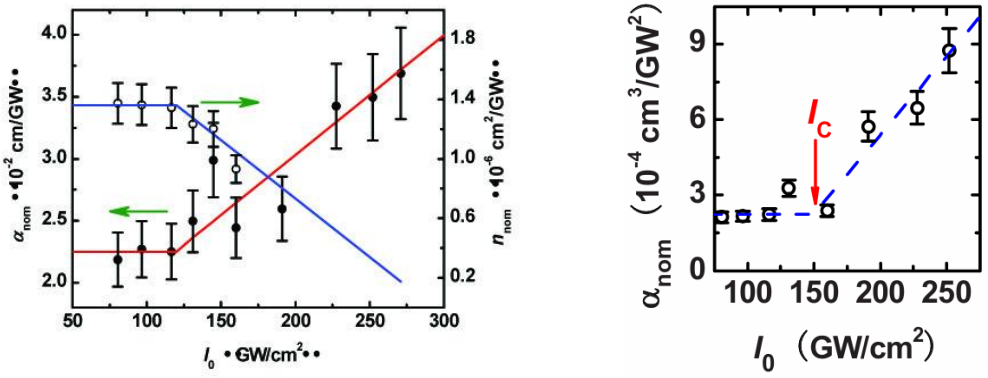

(a) (b)

245TN **245TA**

(c)

Figure 2.6 (a) Intensity dependence of effective 2PA coefficient and nominal nonlinear refraction index coefficient for **245TN**, respectively. (b) Intensity dependence of effective 3PA coefficient for **245TA**. (c) Scheme of molecular structures of **245TN** and **245TA**.

Note. Z-scan experiment was performed using 210 fs- and 350 fs pulse lasers at 780 nm for compound **245TA** and **245TN**, respectively. I_C represent critical intensity. Figures (a) and (b) adapted from reference (Gu *et al.*, 2009b) and (Gu *et al.*, 2010a), respectively.

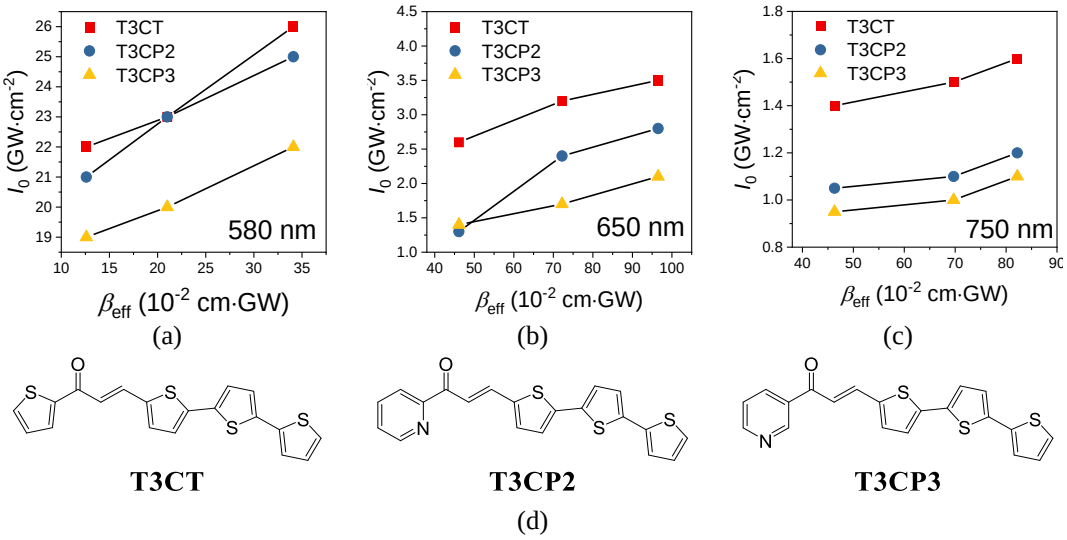

Figure 2.7 Effective RSA coefficient which determined through 190 fs pulse laser Z-scan experiments at (a) 580, (b) 650, and (c) 750 nm, and scheme for molecular structures of **T3CT**, **T3CP2**, and **T3CP3**.

Note. Z-scan experiment was performed using 190 fs pulse laser. Data of figures (a–c) adapted from reference (Jia *et al.*, 2020).

2.2.2 Molecular Aggregations and Environmental Factors

Environmental conditions, such as solvent polarity, concentration, and phase of the compound, significantly influence NLO properties by altering the electronic environment around molecules. For instance, studies have demonstrated that an increase in solvent polarity enhances NLO responses in compounds such as 4'-ethoxy-4-methoxy-chalcone (**EPMP**) (Mathew *et al.*, 2024b), benzodioxol chalcone (**BZDP**) (Mathew *et al.*, 2023), and 3,4,2',4'-tetrahydroxychalcone (**2DHP**) (Mathew *et al.*, 2024a) through the solvatochromic method (Figure 2.8). In terms of concentration effects, Patil *et al.* (2019) observed a two-fold increment in the cubic hyperpolarizability in anthracene-based chalcone (**NANC**) (Figure 2.9) when the concentration was raised from 1 mM to 5 mM in *N*, *N*-dimethylformamide (DMF) solution. This enhancement was attributed to the aggregation effects occurring in more concentrated solutions. Similarly, significant amplification of two-photon absorption

(σ_{2PA}), approximately 30 times greater than that of the monomer, was reported in tetrakis(4-sulfonatophenyl)porphyrin diacid (**H_4TPPS^{2-}**) in acidified water, which contained aggregates (Collini *et al.*, 2005). The impact of aggregation effect on NLO properties has also been explored through quantum-chemical calculations. DFT models have predicted that different dimer arrangements of 5-methyl-4'-nitrochalcone (**3MPNP**) result in variations in dipole moments and cubic hyperpolarizabilities (Valverde *et al.*, 2018b). Specifically, an antiparallel π-stacking dimer reduces the dipole-dipole interactions, leading to a reduction of cubic hyperpolarizability, while a head-to-tail dimer enhances cubic hyperpolarizabilities as a result of strong dipole-dipole interaction. These findings align with earlier studies on 4-nitroaniline (**PNA**), where the in-line head-to-tail dimer configuration was identified as optimal for increasing NLO properties compared to its monomer (Figure 2.10) (Datta *et al.*, 2003). The impact of compound phase on NLO properties was demonstrated through a comparison of two-photon absorption cross-section for a series of quadrupolar π-conjugated dyes (**QP1**–**QP8**) through molecular dynamics in the gas phase and condensed phase (Figure 2.11) (Zeman *et al.*, 2022). The study found that intermolecular stacking arrangements resembling J-aggregates are associated with enhanced 2PA activity, whereas H-aggregates correspond to reduced 2PA activity (Figure 2.12).

In addition to π-stacking interactions and hydrogen bonding, halogen bonding has been identified as a significant contributor to NLO behavious. Computational studies of the static second-order NLO susceptibility ($\chi^{(2)}$) for crystal structures of 2-iodo-3-hydroxypyridine revealed an inverse linear correlation between NLO response and the intermolecular I···I halogen bond length (Yushina *et al.*, 2018). Halogen atoms can direct molecular crystallization into non-centrosymmetric space groups, which are

favourable for NLO activity. In contrast, molecules bearing hydrogen-bonding functionalities and hydrophobic alkyl or aryl substituents often adopt centrosymmetric packing. This occurs due to the antiparallel alignment of molecular dipoles—leading to charge cancellation between neighbouring domains—as well as the general tendency for close packing in molecular crystals, where bumps fit into hollows (Saha *et al.*, 2006).Virkki *et al.* (2015) proved that halogen bonding greatly enhances the NLO response in poled supramolecular polymer systems. They reported that halogen-bonded supramolecular systems surpass their hydrogen-bonded counterparts, even when both types of interactions prosses comparable bond strengths.

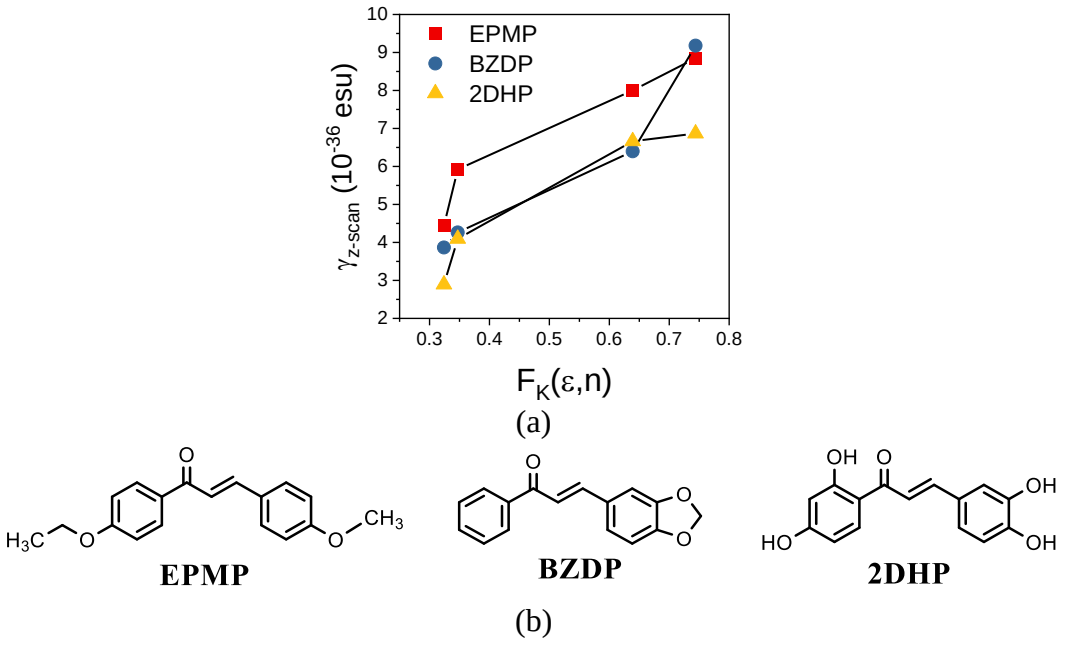

Figure 2.8 (a) Obtained cubic hyperpolarizability through Z-scan experiment against solvent polarity function of Kawski-Chamma-Viallet and (b) scheme for molecular structures of **EPMP**, **BZDP**, and **2DHP**.

Note. Z-scan experiment was performed using 5 ns pulse laser at 532 nm. Selected solvents are dimethyl sulfoxide (DMSO), acetone, toluene, and carbon tetrachloride (CCl_4). Data of figure (a) adapted from references (Mathew *et al.*, 2024a; Mathew *et al.*, 2024b; Mathew *et al.*, 2023).

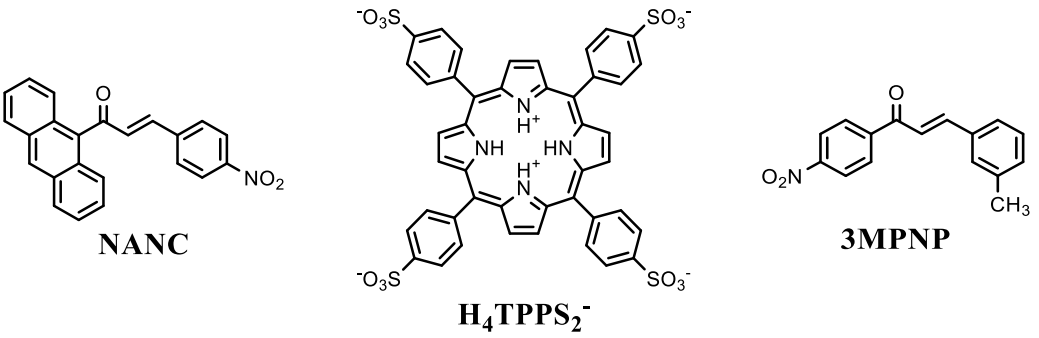

Figure 2.9 Scheme for molecular structures of **NANC**, **H_4TPPS^{2-}** and **3MPNP**.

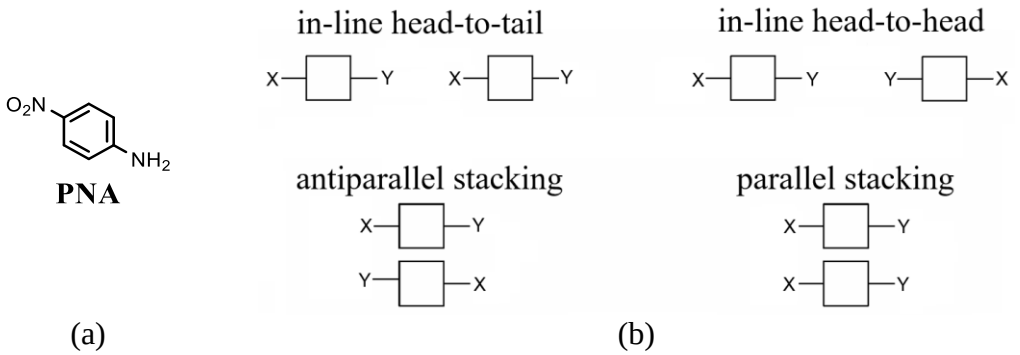

(a) (b)

Figure 2.10 (a) Scheme for molecular structure **PNA** and (b) four different dimer configurations.

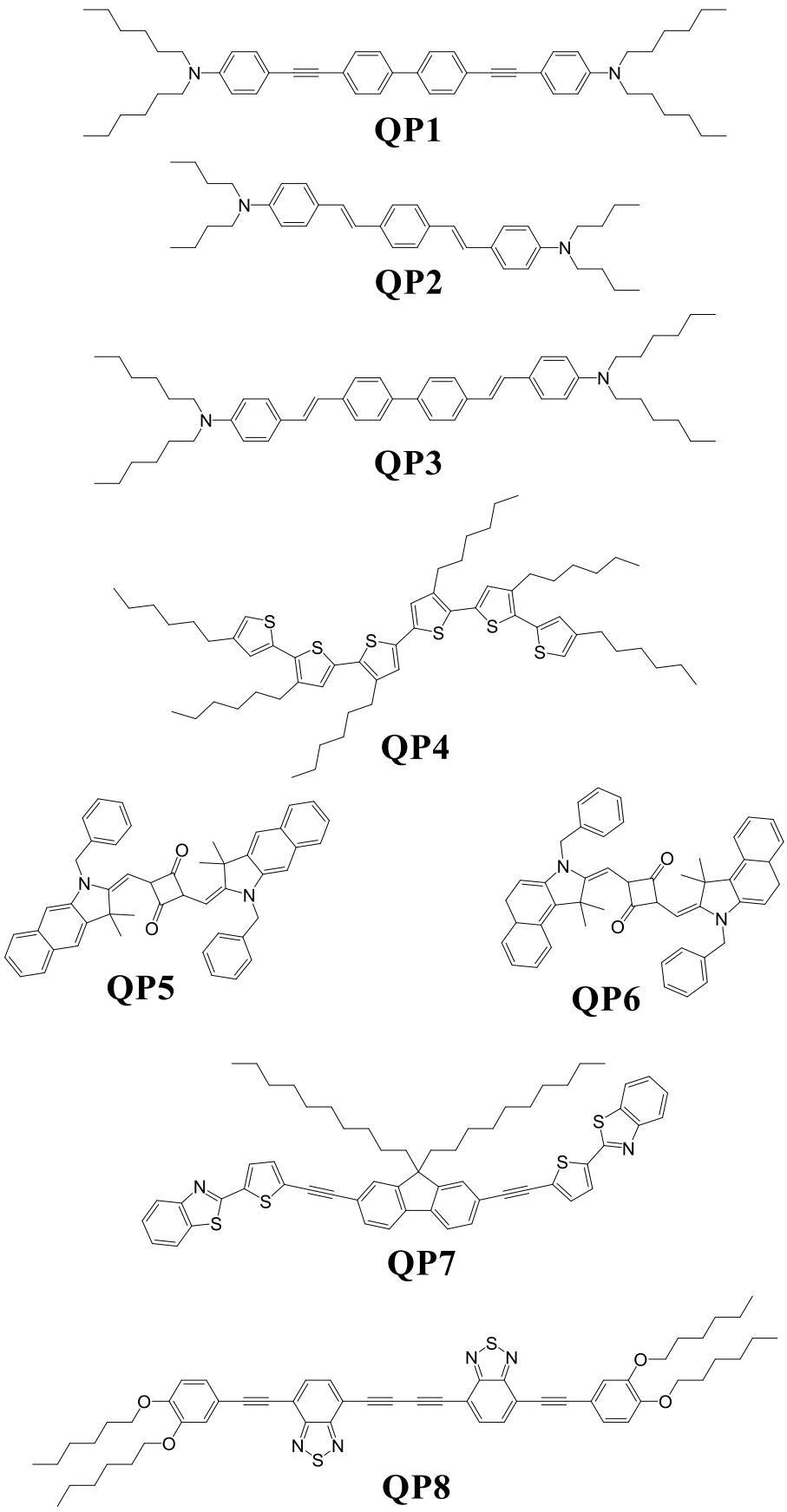

Figure 2.11 Scheme of reported quadrupolar π-conjugated dye molecules by Zeman *et al.* (2022).

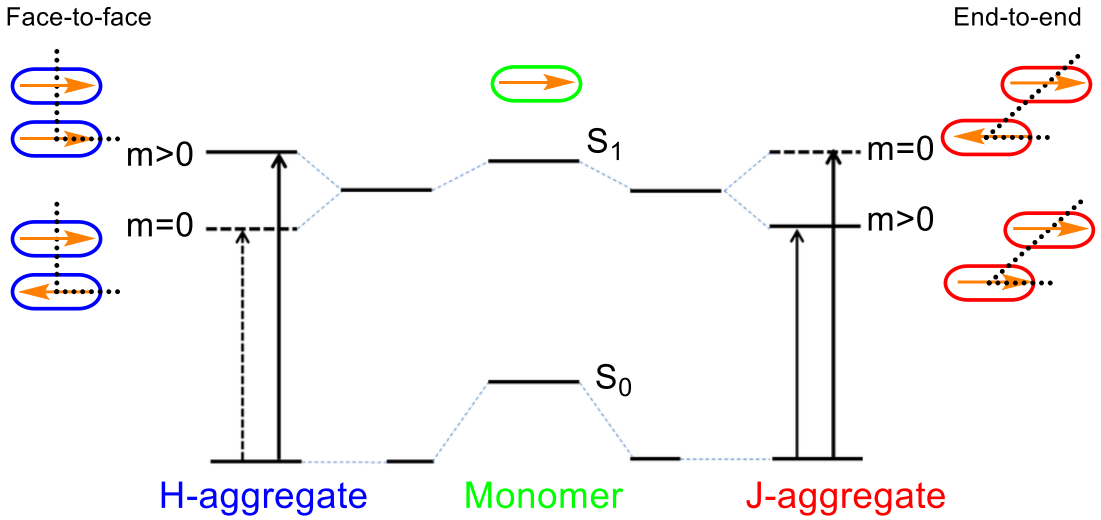

Figure 2.12 Scheme presentation of energy level of molecular monomer, H-aggregate (face-to-face configuration) and J-aggregate (end-to-end configuration) formation.

Note. Optically allowed transition when m greater than zero, where m represents the sum of transition dipole moments (orange arrow).

2.2.3 Role of Structural Determinants in NLO Responses

Structural characteristics are permanent features of the molecule, providing a predictable basis for NLO properties. Structural factors allow for the rational design of molecules with tailored optical performance. The best chromophore to render the material non-linear can be exploited by deciphering basic structure-property relationships that instruct synthetic chemists on the kinds of structures correlated with a large NLO response.

2.2.3(a) Conjugation

Conjugation facilitates the delocalization of π-electrons across the molecular backbone, enhancing intramolecular charge transfer and resulting in strong NLO responses. Research has consistently demonstrated that increasing the effective number of π-electrons (twice the number of double bonds) in a system improves electron flow, thereby enhancing the material's overall NLO properties (de Wergifosse

et al., 2011; Klimenko *et al.*, 2009), specifically, the static quadratic hyperpolarizability (β), cubic hyperpolarizability (γ) and 2PA cross-section in polymer and oligomer increase according to the power law of n^c, where n represents the number of π-electrons and c is the exponent (Figures 2.13–2.15) (Kuzyk, 2009). Incorporating π-bridges with aromatic rings was discovered to further strengthen NLO responses. Momicchioli *et al.* (2014) studied theoretically a more than 1.1-fold magnification of β in a Michler's ketone analogue (also known as bis-chalcone) (**KM1**) with respect to a similarly sized ketocyanine (**KC3**) at the converged SOS level (Figure 2.16). Similar enhancements were observed in a comparison of the 2PA cross-section between stilbene, fluorene and biphenyl (Figure 2.17) (Morel *et al.*, 2001) and in the β between stilbene derivative and biphenyl derivative (Figure 2.18) (Paschoal *et al.*, 2013; Tam *et al.*, 1991). These modifications increase π-electron delocalization while simultaneously promoting a more planar molecular structure, which is crucial for maintaining uniform electron distribution and optimizing the NLO response. Experimental work through Hyper-Rayleigh scattering (HRS) spectroscopy on chalcone and stilbene derivatives by Rawal *et al.* (2016) demonstrated that cross-conjugated molecules can achieve NLO properties tantamount to fully conjugated molecules (Figure 2.19). This finding highlights that structures featuring multiple donors (acceptors) linked to a single acceptor (donor), resembling V-shaped or star-shaped molecules (Figure 2.20) (Kuzyk *et al.*, 2013a; Lytel *et al.*, 2013), could be a highly effective strategy for optimizing NLO properties.

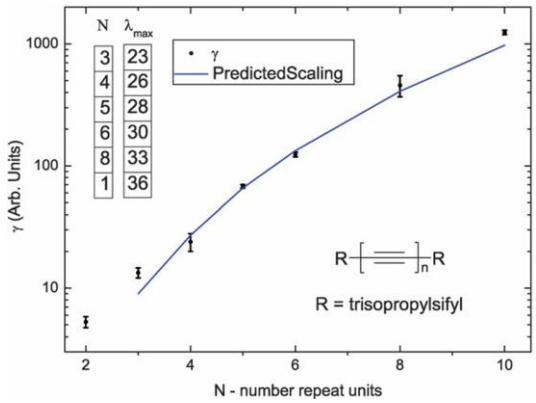

Figure 2.13 The cubic hyperpolarizability of a series of polyyne oligomers against number of repeat units (points with error bars).

Note. Figure adapted from reference (Kuzyk, 2009; Slepkov *et al.*, 2004).

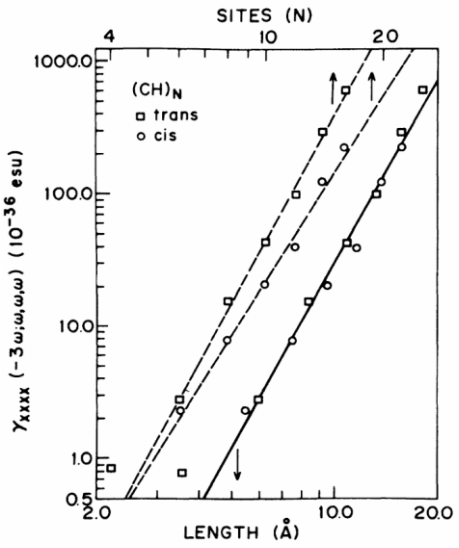

(a)

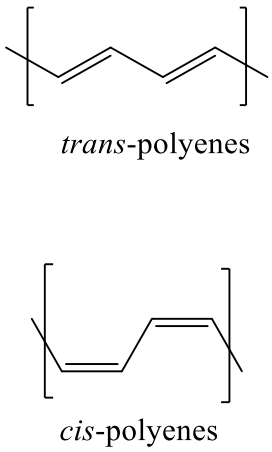

(b)

Figure 2.14 (a) Log-log plot THG cubic hyperpolarizability ($\gamma_{xxxx}(-3\omega;\omega,\omega,\omega)$) against the number of carbon sites *N* (upper scale) and the length *L* (lower scale) and (b) scheme of molecular structures for *trans*- and *cis*-polyenes.

Note. Figure (a) adapted from reference (Heflin *et al.*, 1988).

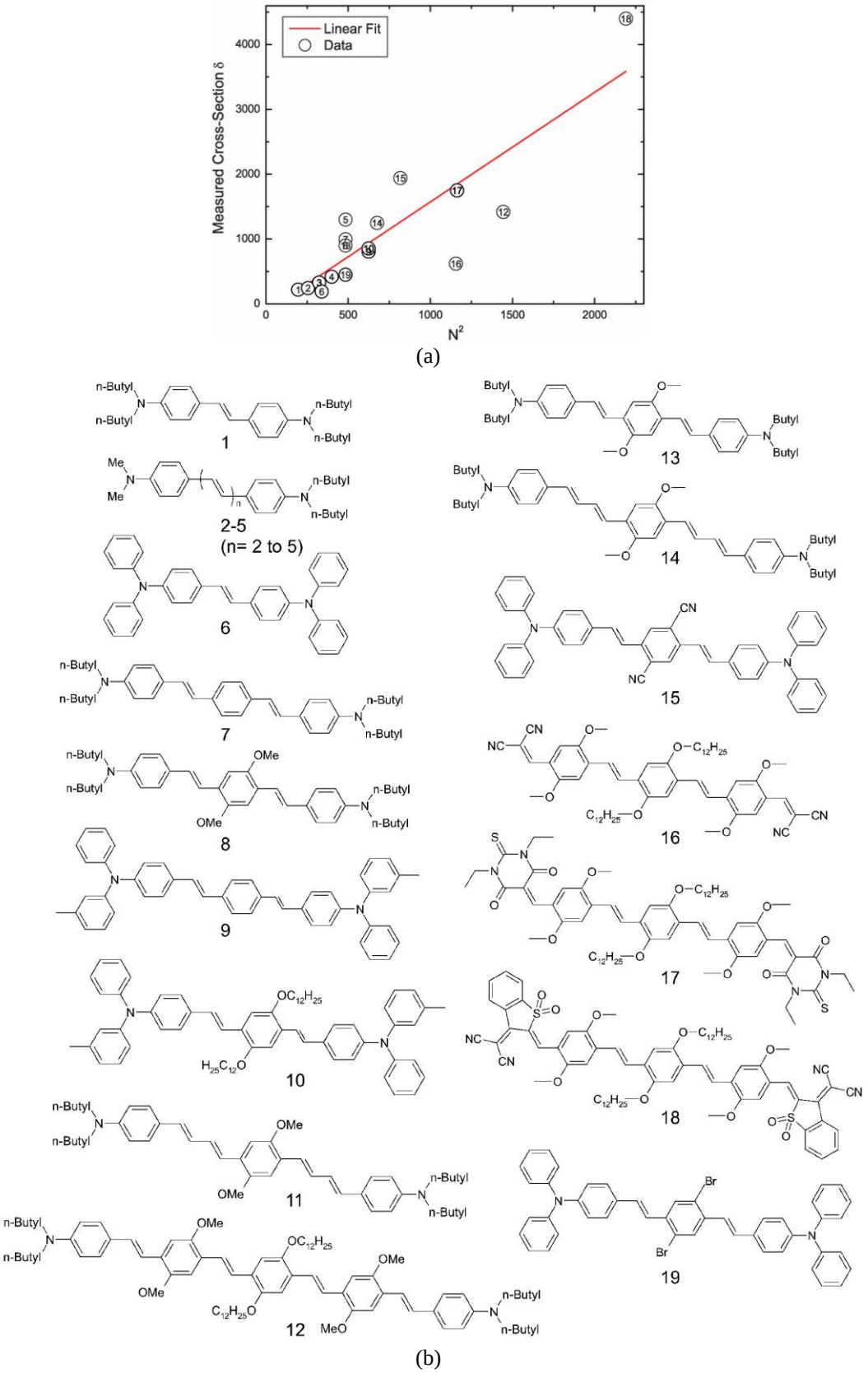

Figure 2.15 (a) The 2PA cross-section against square of number of electrons and (b) scheme of the reported molecular structures by Rumi *et al.* (2000) and Albota *et al.* (1998).

Note. Figures (a–b) adapted from reference (Kuzyk, 2009).

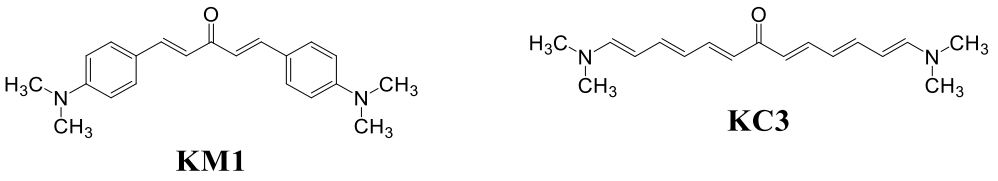

Figure 2.16 Scheme for molecular structures of **KM1** and **KC3**.

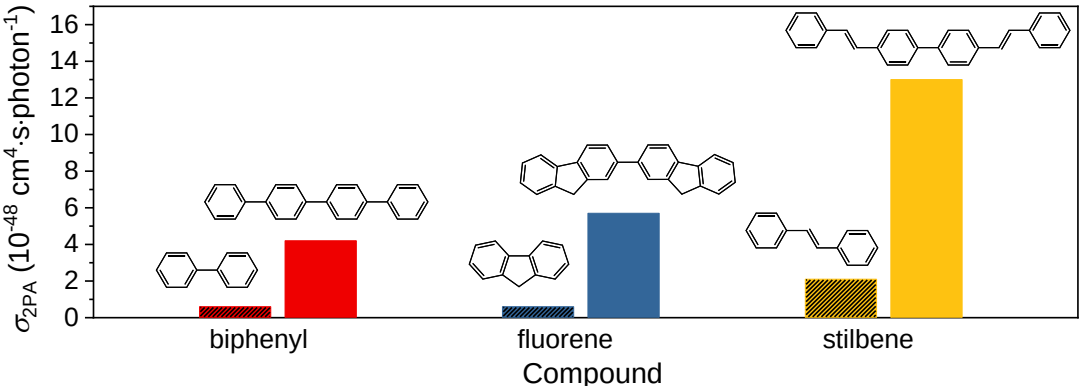

Figure 2.17 Theoretical 2PA cross-section of biphenyl, fluorene stilbene monomer and dimer which computed through semi-empirical quantum chemistry calculations.

Note. Data adapted from reference (Morel *et al.*, 2001).

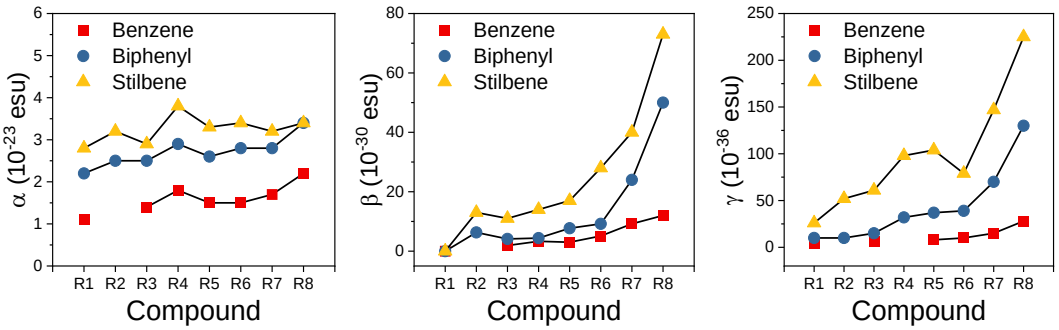

(a)

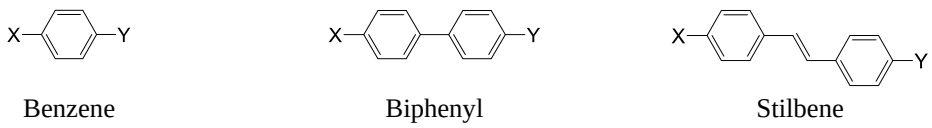

R1:	H	&	H	R4:	NO_2	&	Br	R7:	NO_2	&	NH_2
R2:	CN	&	OH	R5:	NO_2	&	OH	R8:	NO_2	&	$N(Me)_2$
R3:	NO_2	&	H	R6:	NO_2	&	OMe				

(b)

Figure 2.18 (a) Experimental NLO results and (b) scheme for molecular structures of benzene, biphenyl and stilbene along with their disubstituted derivatives.

Note. Data of figure (a) adapted from reference (Cheng *et al.*, 1991a; Cheng *et al.*, 1991b).

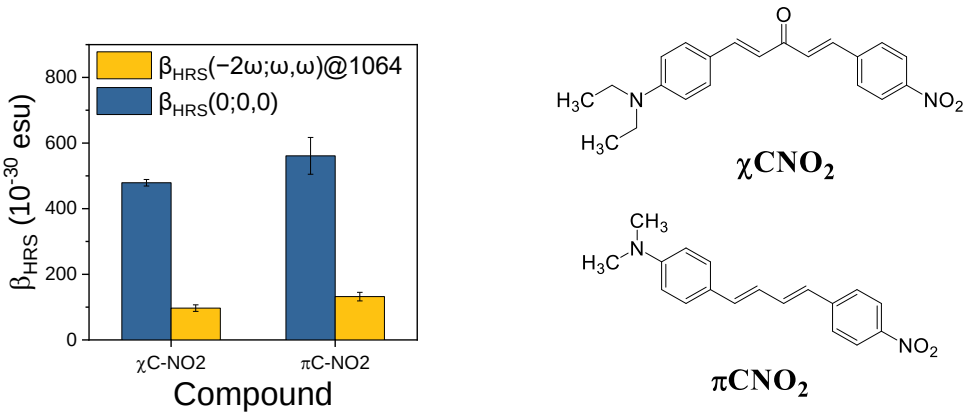

(a) (b)

Figure 2.19 (a) Experimental quadratic hyperpolarizability values measured at 1064nm and extrapolated to zero frequency and (b) scheme for molecular structures for χCNO_2 and πCNO_2.

Note. HRS experiment was performed using pulsed laser and calibrated using 4-nitroaniline in $CDCl_3$ solution as reference standard. Data of figure (a) adapted from reference (Rawal *et al.*, 2016).

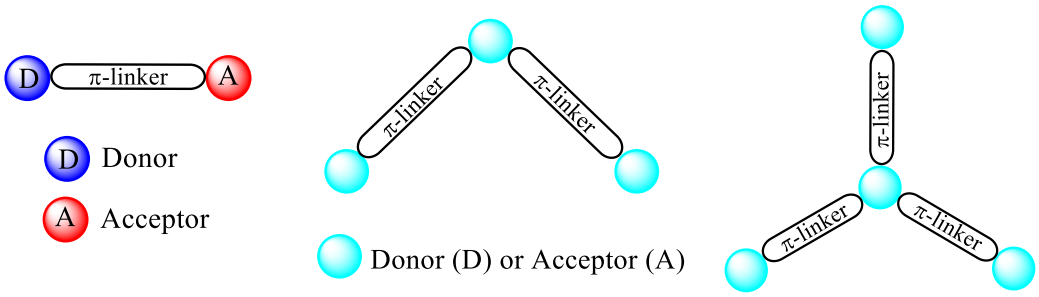

(a) linear (b) V-shaped (c) Star-shaped

Figure 2.20 Schematic representation of the (a) linear, (b) V-shaped and (c) star-shaped centrifugal push-pull molecules.

Note. A V-shaped molecule with symmetric terminal groups and an asymmetric central atom typically behaves like a quadrupolar molecule, while a star-shaped molecule with symmetric terminal groups and an asymmetric central atom might exhibit an octopolar nature.

2.2.3(b) Planarity and Conformation

Similar to stilbene, chalcone typically adopts a planar conformation under normal conditions, which allows for better overlap of molecular orbitals, thus helping preserve charge transfer pathways and contributing to its significant NLO response (Chen *et al.*, 2023; Resan *et al.*, 2020). This planar structure is primarily due to chalcone's preference for the *trans*-(*s-cis*) configuration with respect to the enone moiety, as it offers greater stability compared to other configurations that may